Aerospace Science and Technology 73 (2018) 10–18

Contents lists available at ScienceDirect

Aerospace Science and Technology

www.elsevier.com/locate/aescte

Characterisation of turbine behaviour for an engine overspeed prediction model

Lucas Pawsey *, David John Rajendran, Vassilios Pachidis

Centre for Propulsion Engineering, School of Aerospace, Transport and Manufacturing, Cranfield University, Bedfordshire, United Kingdom

ARTICLE INFO

Article history:
Received 15 February 2017
Accepted 20 November 2017
Available online 28 November 2017

ABSTRACT

This paper focuses on the characterisation of turbine overspeed behaviour to be integrated into an engine overspeed model capable of predicting the terminal speed of the high pressure turbine (HPT) in the event of a high pressure shaft failure. The engine considered in this study features a single stage HPT with a shrouded contra-rotating rotor with respect to the single stage intermediate pressure turbine (IPT). The HPT performance is characterised in terms of torque and mass flow function for a range of expansion ratios at various non-dimensional rotational speeds (NH), up to 200% of the design value. Additionally, for each HPT expansion ratio and NH, the change in capacity of the downstream IPT, for different IPT non-dimensional rotational speeds (NI), also needs to be characterised due to the extremely positive incidence angle of the flow from the upstream rotor. An automated toolkit is developed to generate these characteristic maps for both the HPT and IPT.

An unlocated high pressure shaft failure will result in rearward movement of the rotor sub-assembly. This causes changes in the rotor tip and rim seal regions, and in the rim seal leakage flow properties. Therefore, in the present work, a high fidelity characterisation of turbine behaviour with the inclusion of tip and rim seals is carried out at three different displacement locations, 0 mm, 10 mm and 15 mm, to improve terminal speed estimation. Furthermore, there is a possibility of damage to the tip seal fins of the HPT rotor due to unbalance in the spool that may result in contact between the rotor aerofoil tip and the casing. Consequently, another set of characteristics are generated with damaged tip fins at each displacement location.

It is observed from the characteristics that the torque of the HPT rotor decreases with increasing NH. The HPT mass flow function initially decreases and then increases with an increase in NH. The IPT mass flow function initially remains similar and then decreases with increase in NH above values of 150%. The HPT rotor torque and IPT mass flow function decrease with rearward movement of the HPT rotor sub-assembly for all values of NH. With worn tip seal fins all parameters mentioned previously are lower than in the nominal undamaged case. The high fidelity characterisation of turbines that follows the sequence of events after a shaft failure, as described in this work, can provide accurate predictions of terminal speed and thus act as a tool for testing design modifications that can result in better management and control of the over-speed event.

© 2017 The Authors. Published by Elsevier Masson SAS. This is an open access article under the CC BY license (http://creativecommons.org/licenses/by/4.0/).

1. Introduction

A shaft failure may lead to the decoupling of the compressor and the turbine mounted on the shaft. The decoupling leads to a situation in which the power produced by the turbine is no longer absorbed by the compressor. However, the expansion of the gases through the turbine rotor does not instantaneously cease at the moment of the shaft breakage owing to the flow of gases in the main gas path, causing the rotor assembly to accelerate. Should it not be restrained in some way, it will reach a critical speed at which permanent plastic deformation may occur, followed by disc burst. Should the bearings be arranged in such a way that the turbine is left without axial constraint following the failure, it will move rearward during the event owing to the axial force acting upon it, termed an unlocated shaft failure. The above sequence of events occurring in the engine is typically termed as a shaft overspeed event. Stringent guidelines on the eventuality of shaft failure and its management are specified in the engine certification requirements [1,2]. Engine certification guidelines specify

* Corresponding author.
E-mail address: l.pawsey@cranfield.ac.uk (L. Pawsey).

https://doi.org/10.1016/j.ast.2017.11.037
1270-9638/© 2017 The Authors. Published by Elsevier Masson SAS. This is an open access article under the CC BY license (http://creativecommons.org/licenses/by/4.0/).

Nomenclature

AS	Automation Script
CCL	CFX Command Language
GCI	Grid Convergence Index
HPT	High Pressure Turbine
HPC	High Performance Computing
IPT	Intermediate Pressure Turbine
NH	HP non-d speed function
NI	IP non-d speed function
MFF	Mass Flow Function
PR	Pressure Ratio
RANS	Reynolds Averaged Navier–Stokes
SST	Shear Stress Transport
ref	reference

that the engine can be deemed safe from shaft failure considerations by either a full scale actual engine test or by analyses that provide detailed descriptions of the likely progression of events following a shaft failure, arising from all possible reasons, along with details of design or flow features that will control or limit the possibility of the shaft failure event in becoming a criticality. Therefore, the development of engine models to understand the response of the engine during a shaft breakage event is of paramount importance. During the overspeed event, engine components can exhibit a wide range of behaviour depending upon the architecture of the engine and the type of failure. Typically the compressor behaviour is dominated by reverse flow, surge or stall. The change in compressor behaviour changes the response of the secondary air system. In the case of an unlocated failure, as studied here, the turbine rotor assembly moves axially rearwards because of unbalanced axial forces. This downstream movement of the turbine results in mechanical interaction between the rotor and the downstream components, and damage to the secondary air system elements in the disc region. Therefore, only a transient engine overspeed model that takes into account the behaviour of the compressors, turbines, secondary air system and mechanical interaction of the rotor with other components can accurately predict the evolution of the rotor speed with time after shaft failure [3–6].

Characterisation of the turbine behaviour during the engine overspeed event, for use in an engine overspeed model for HP shaft failure, is discussed in the present paper. The HP and the IP turbine parameters that influence the terminal speed of the HP rotor, at various operating conditions, need to be specified in the engine model as characteristic maps. In the HPT, the rotor aerofoil torque and the mass flow function, at different expansion ratios and NH, influence the terminal speed. Since, during the progression of the over-speed event the NH may attain values in excess of 160% of the design value because of the unloading of the turbine, possibility of surge in the compression system and combustion instabilities that lead to a reduction in the turbine entry temperature, overspeed characterisation should be carried out up to 200% of the design NH value. Therefore, a traditional characteristic map of the HP torque and mass flow function for an extended range of NH is required. In the case of the IPT, the change in the IP turbine mass flow function corresponding to each NH and HPT pressure ratio, needs to be mapped since the IPT throttles the HPT and fixes its operating point. This change in IPT capacity needs to be obtained for different values of NI. Therefore, the IPT characteristic is linked to the HPT characteristic during an overspeed event. A typical overspeed model imposes conditions of equilibrium in the engine to pick up the operating point of each turbine from operating maps and solves for the evolution of rotor speed with time. The only public domain literature available, published outside of Cranfield, regarding the development of engine overspeed model is the work by M. Haake et al. [7]. The model predicts the terminal speed of the overspeeding rotor by the use of main gas path component characteristics. The turbine characteristics are generated using a generic performance synthesis program, and does not explicitly model the events occurring in the turbine after the shaft failure event.

In the present work, a high fidelity characterisation of the turbine behaviour is presented for application in an engine overspeed model for the HP spool of a typical gas turbine engine. The methodology for characterisation includes explicit modelling of the events that occur during an unlocated shaft failure like axial displacement of the HP rotor sub-assembly, damage to the rotor aerofoils, and change in the properties of the leakage flow that interacts with the expanding gases in the turbine flow path. The change in the performance parameters of the turbine for nominal operating conditions at different axial displacements have been studied in detail by the authors using integrated aerodynamic, secondary air system model and structural analyses [8]. Additionally the characterisation is also attempted for the case in which the shroud fins of the rotor tip gets damaged because of an unbalance triggered in the rotor assembly after shaft failure. The effect of the damaged or worn tip fins on the on the turbine performance parameters for nominal operating conditions at different axial displacements have also been explored by the authors using a similar integrated methodology [9]. The need for characterisation of turbines at different axial displacements and for different tip seal configurations results in a large number of operating points for which the flow solution needs to be carried out. Therefore an automation framework is developed to obtain the overspeed maps of the turbine in the present work. This kind of high fidelity characterisation of turbines can greatly improve the accuracy of prediction of the rotor terminal speed. The methodology followed for the characterisation and the discussion of the trends in turbine parameters at different non-dimensional speeds are discussed in this paper.

2. Methodology

The turbine configuration considered in the present study consists of a single stage shrouded HPT that is contra-rotating with respect to a single stage downstream IPT stage. The rearward axial displacement of the HP rotor following an unlocated shaft failure is predicted by the use of a validated thermo-mechanical friction model developed on the basis of non-linear structural dynamic analyses carried out using LS-DYNA [10]. This rearward movement of the HP rotor sub-assembly changes the axial distance between the HP rotor and stator aerofoil, increases the tip clearance and damages portions of the HP rotor aerofoil that comes into contact with the downstream IPT hub platform casing. The HP rotor considered in the present study has a flared shrouded rotor tip that forms a seal with a three step casing that bridges the flare angle. This geometric arrangement of the of the turbine configuration is such that no significant changes in the tip clearance arises until a rearward axial displacement 10 mm from the initial position of the rotor. Further, it is observed that beyond an axial displacement of 15 mm, large portions of the rotor aerofoil sustain damage, and so axial displacement was limited to 15 mm. Therefore, the characteristics of the turbine are generated for the un-displaced rotor, and for the rotor at 10 mm and 15 mm displacements respectively.

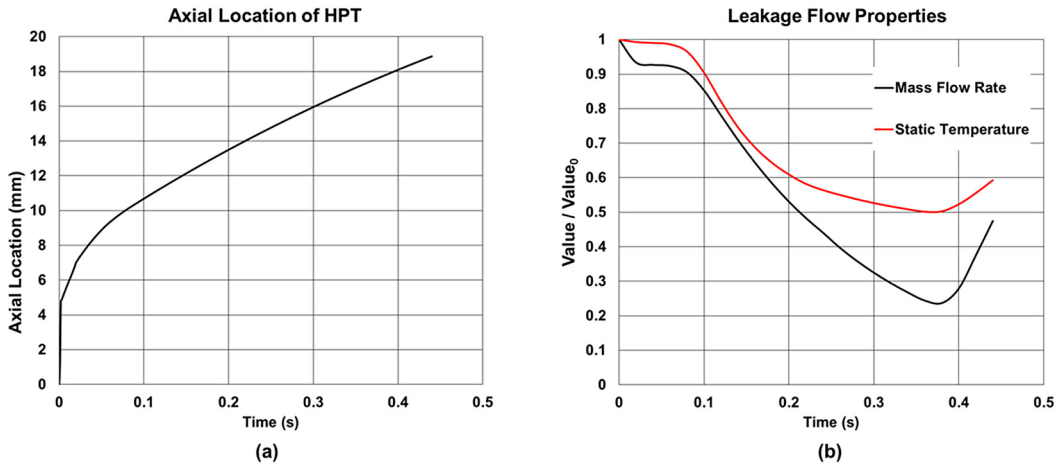


Fig. 1. (a) Axial location vs time from friction model. (b) Leakage flow rate and temperature vs time from secondary air system model.

The damage in the rotor aerofoil at each axial displacement is obtained from structural contact analyses carried out using LS-DYNA. The rearward movement also results in a change in the boundary conditions of the leakage flow that interacts with the main flow through the stator–rotor gap in the hub region of the flow path that is typically called the rim seal. The change in the rim seal gap and the properties of the leakage flow with axial displacement influences the turbine behaviour to a significant extent, and is therefore explicitly modelled for the characterisation. The change in the properties of the leakage flow is obtained from a validated transient secondary air system model [11,12]. The evolution of axial displacement with time obtained from the friction model, and the change in the leakage flow properties obtained from secondary air system model are shown in Fig. 1.

The objective of the engine overspeed model is to predict the speed of the rotor with time. Therefore, the generation of turbine characteristics at different axial displacements, and then interpolating the characteristics in the appropriate axial displacement range holds the potential for greatly increasing the accuracy of the prediction of the rotor terminal speed.

Additionally, a design modification in which an unbalance is triggered in the HP rotor and results in damage to the fins in the shroud rotor tip seal after shaft failure is explored. Therefore, the degradation in the turbine performance with worn fins at different axial displacements is also characterised to quantify the effect of the design modification. The characteristics of the HPT and IPT are generated by 3D Reynolds Averaged Navier–Stokes (RANS) analyses by calculating the turbine performance parameters at each expansion ratio and non-dimensional speed functions.

3. Computational domain and boundary conditions

The extent of characterisation at different axial displacements and for different tip seal configurations are shown in Fig. 2. In order to generate the flow solutions for the different cases, two different computational domains, one for the HPT, and another for the IPT are defined at each axial displacement location i.e. 0 mm, 10 mm and 15 mm. Furthermore, another set of computational domains with worn fins at the HP rotor tip seal are also considered at each axial displacement location.

The computational domain of the HPT includes the HP stator with the trailing edge coolant flow slot, HP rotor with the rim seal and the tip seal, and the downstream IP stator. The IP stator is included in the HP turbine computational domain to impose the appropriate conditions to which the flow in the HPT is expanding and to directly provide the mass flow function of the IPT corresponding to each HPT operating condition. The IPT computational domain consists of the IP stator and the IP rotor. Grids of high quality indices are generated for each of the computational domains. The sizes of the grids are finalised on the basis of a grid sensitivity study based on Richardson's extrapolation method with a numerical error, at maximum NH speed, of not more than 0.7% for the IPT, and 0.5% for the HPT in all parameters of interest [13]. At nominal conditions these numerical errors reduce to below 0.3%.

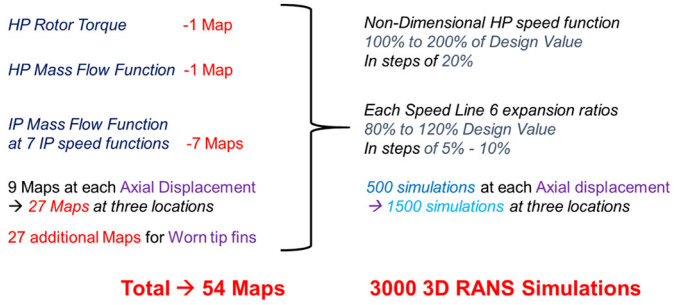


Fig. 2. Schematic showing extent of characterisation and flow simulations.

The flow conditions at the HP rotor outlet for each operating condition of the HPT are mapped on to the inlet of the IPT. Therefore, the expansion ratio of the IPT at a particular non-dimensional speed function for the flow exiting from the HPT can be obtained. The non-dimensional speed function of the IPT is kept constant for all the different operating points of the HPT by updating the mechanical speed of the IPT based on the outlet total temperature of the HP rotor. The boundary conditions to obtain the flow solution in the HPT are profiles of total pressure, total temperature, and flow angle at the HP stator inlet, mass flow rate and temperature of trailing edge coolant flow and rim seal leakage flow, mechanical speed of the HP rotor, and static pressure at the outlet of the downstream IP stator. The static pressure at the outlet is varied to change the expansion ratio of the turbine, and the mechanical speed of the rotor is varied to change the non-dimensional speed function of the turbine. The computational domain at each axial displacement is evaluated for similar boundary conditions in the main flow path. However, the flow properties of the secondary air system flows are updated from the results obtained from the transient secondary air network model. Similar boundary conditions are used to evaluate the characteristics for the worn fins in the tip seal. Boundary conditions of the IPT domain are profiles of total temperature, total pressure, radial and tangential flow angles at the inlet of the IP stator, and mass flow rate at the outlet of the IP rotor. Boundary conditions for the IP computational domain

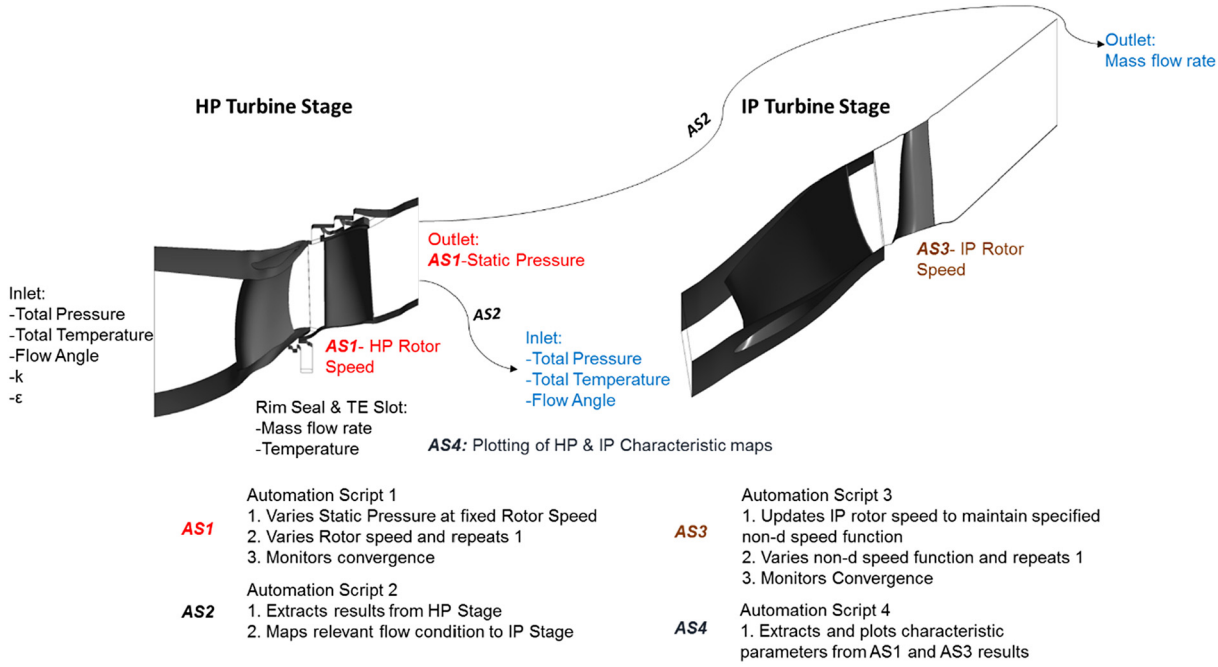


Fig. 3. Automation scripts for characterisation of HP and IP turbines.

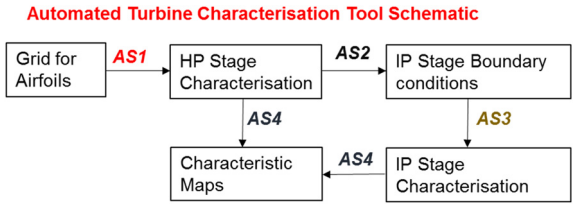


Fig. 4. Automation tool schematic for characterisation.

are obtained from the HP rotor outlet at each condition. The mechanical speed of the IP rotor is specified based on the inlet total temperature to obtain a particular non-dimensional speed function of the IPT stage. The IPT domain is evaluated for each operating point of the HP turbine at different axial displacements to obtain the behaviour of the IP turbine that is linked to the overspeeding HP rotor. As indicated in Fig. 2, characteristics are generated for 7 IP speeds across a normal operating range.

4. Automation framework and flow solution

In the present work, the 3D RANS solution for both the HP and the IPT computational domains is carried out using commercial CFD solver, ANSYS CFX [14]. The steady RANS equations are solved in a fully implicit manner by using higher order numerical resolution schemes for both the conservation and turbulence quantities. The effect of turbulence is modelled using k–ω Shear Stress Transport (SST) model [15]. The large number of flow simulations and the mapping of boundary conditions between the computational domains necessitate the requirement of an automation framework that holds the potential for reduction of the number of man hours required for the characterisation of the turbines in over-speed. An automation framework as shown in Figs. 3 and 4 is developed using CFX Configuration Language (CCL) and MATLAB in the present work.

The automated turbine characterisation toolkit works on the basis of four Automation Scripts (AS). AS1 is executed from a MATLAB code that uses CCL to modify NH and HP rotor outlet static pressure to characterise the HPT. The AS2 is a MATLAB code that automatically post-processes the results from the HPT analyses from CFX-Post and maps the total pressure, total temperature, flow angle and mass flow rate to the IPT inlet and outlet planes. AS3 is a CCL file that calculates the speed of the IP rotor from the IP inlet properties to obtain the required IPT non-dimensional speed function (NI), and characterises the behaviour of the IP turbine. AS4 extracts and plots the characteristic parameters from the flow analyses results. The AS1 and AS3 scripts that characterise the individual turbines also monitor the convergence of the individual flow domain solution and uses the solution from one point as the initial condition for other points. All the automation scripts are run from a master MATLAB script that integrates the execution of the individual scripts. The solution is carried out in a High Performance Computing (HPC) facility at Cranfield University. The usage of the automation scripts has resulted in the entire characterisation of both the turbines at different axial displacements and tip configurations to be completed within 9 days. This represents a leap from traditional manual characterisation of turbines that typically takes a month for each configuration.

5. Results and discussion

The results from the array of analyses at different rearward axial displacements of the HPT configuration are post-processed to extract the main parameters of interest for the engine overspeed model, namely the rotor aerofoil torque and the mass flow function. The results are presented in terms of turbine characteristic maps that show the variation of the parameters with turbine expansion ratios for a range of non-dimensional speed functions. For each of the operating points of the HPT from the above characteristic map, the variation of the swallowing capacity with the expansion ratio of the downstream IPT, at a fixed non-dimensional speed function of the IP rotor, is obtained from the solution of the IPT computational domain. These values are then plotted as a characteristic map of the IPT for a particular IP rotor non-dimensional speed function, showing variation of the IPT mass flow function with expansion ratio for different non-dimensional speeds of the HPT. Therefore for each axial displacement configuration a total of three characteristic maps, two for the HPT, and one for the IPT are generated, making a total for nine maps for the three axial displacement locations. The above set of characteristic maps are then

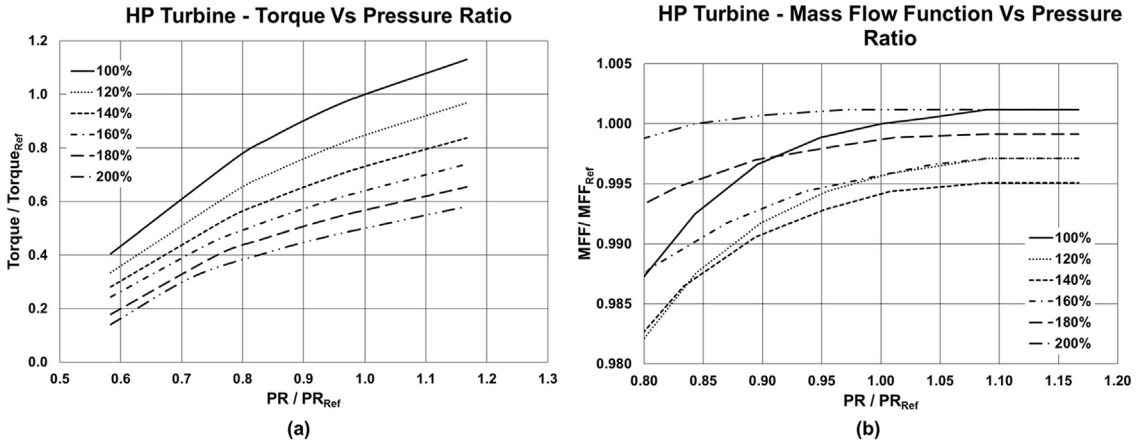


Fig. 5. HPT characteristic maps – (a) torque vs expansion ratio. (b) Mass flow function vs expansion ratio – for different non-dimensional speed functions.

generated for the case in which the fins in the shroud tip seal of the rotor are damaged for different axial displacement cases.

The characteristic maps of the undisplaced HP turbine configuration with no damage to the shroud tip seals are taken as the baseline for comparison with the maps at the other two axial displacement locations i.e. 10 mm and 15 mm, and for the maps generated with the worn fins in the rotor shroud tip seal. Firstly, the change in flow behaviour at different non-dimensional speed functions are discussed for the case of the undisplaced configuration, and thereafter the variation of the other configurations with respect to the baseline is discussed.

5.1. Characteristics of the undisplaced configuration

Typical changes in the trends of the HP rotor aerofoil torque, HPT and IPT mass flow functions at different non-dimensional speed functions are explained in this section using the results for the undisplaced configuration. Characteristic maps of the HPT and the IPT for the undisplaced configuration are shown in Figs. 5 and 6 respectively. In the characteristic maps, the different speed lines are shown as percentages of the design non-dimensional speed function of the HPT rotor. The Mass Flow Function (MFF) is defined on the basis of the turbine inlet mass flow, average inlet total temperature and average inlet total pressure. The torque, Pressure Ratio (PR), and MFF values in the map are normalised with respect to a reference value corresponding to a specific operating point in the engine envelope. It is also to be noted that the speed lines in the IPT characteristic correspond to the non-dimensional speed functions of the HPT rotor, and the entire map shown here corresponds to a single non-dimensional speed function of the IP rotor at the design value. The PR in the IPT map is the expansion ratio of the IPT for the gas expanding from the HPT exit when the IP rotor is operating at a particular non-dimensional speed function value.

It can be observed from the HPT maps that at a specific non-dimensional speed function, as the expansion ratio of the HPT increases, the torque produced by the rotor aerofoil increases. Additionally, as the non-dimensional speed function increases the torque produced by the rotor aerofoil decreases. This behaviour is typical of turbines, because as the expansion ratio of the turbine stage increases, the work output of the turbine increases, and consequently the torque of the rotor blades also increases because the angular velocity of the rotor remains the same. Further, as the non-dimensional speed function of the turbine increases, the angular velocity of the rotor increases, but there is no significant change in the work output of the turbine because of the similar expansion ratio across the turbine stage at different speed functions. Therefore, the torque of the rotor aerofoil decreases with increase

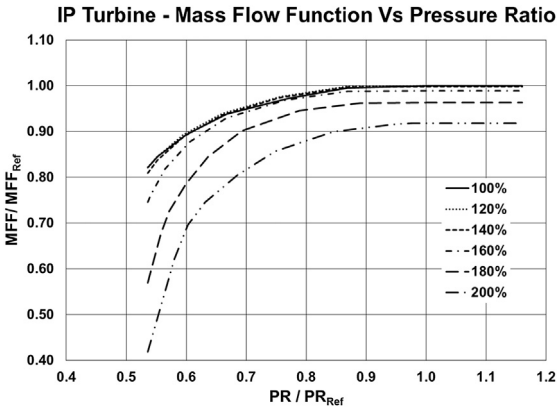


Fig. 6. IPT mass flow function vs expansion ratio – for different HPT non-dimensional speed functions.

in non-dimensional speed function. It is observed that the torque produced by the rotor aerofoil at 200% non-dimensional speed is nearly half that of the torque produced at the nominal condition. It can be observed from the trend of each speed line in the characteristic that at very low expansion ratios, the torque output from the turbine will become zero. It is also observed that the zero torque expansion ratio in the case of higher non-dimensional speed functions are not significantly different from the other speed lines. This is because at very low expansion ratios the turbine is not producing significant amounts of work at any non-dimensional speed line, and consequently the torque produced is also low for all speed lines. The exponential nature of turbine power delivery with expansion ratio is responsible for the higher differences in the torque at higher expansion ratios for different speed lines.

The variation of mass flow function of HPT with expansion ratio shows a typical behaviour at any fixed non-dimensional speed function, i.e. as the expansion ratio increases the mass flow function increases until it reaches the choking value of mass flow and remains constant. However, an interesting trend is observed in the trend of the mass flow function values with non-dimensional speed functions near the normalised pressure ratio value of one. It is observed that the HPT MFF reduces with increasing NH up to 140%. Between 140% and 200% NH the MFF increases back to the capacity seen at 100% NH by the time it reaches 200% NH. The reason for this observed trend is the change in the static pressure field at the inlet plane of the rotor with increase in the angular velocity of the rotor. As the angular velocity of the rotor increases, the value of the relative inlet velocity to the rotor decreases until it reaches a minimum value at a non-dimensional speed function of 140%, at which point the relative inlet velocity to the rotor is

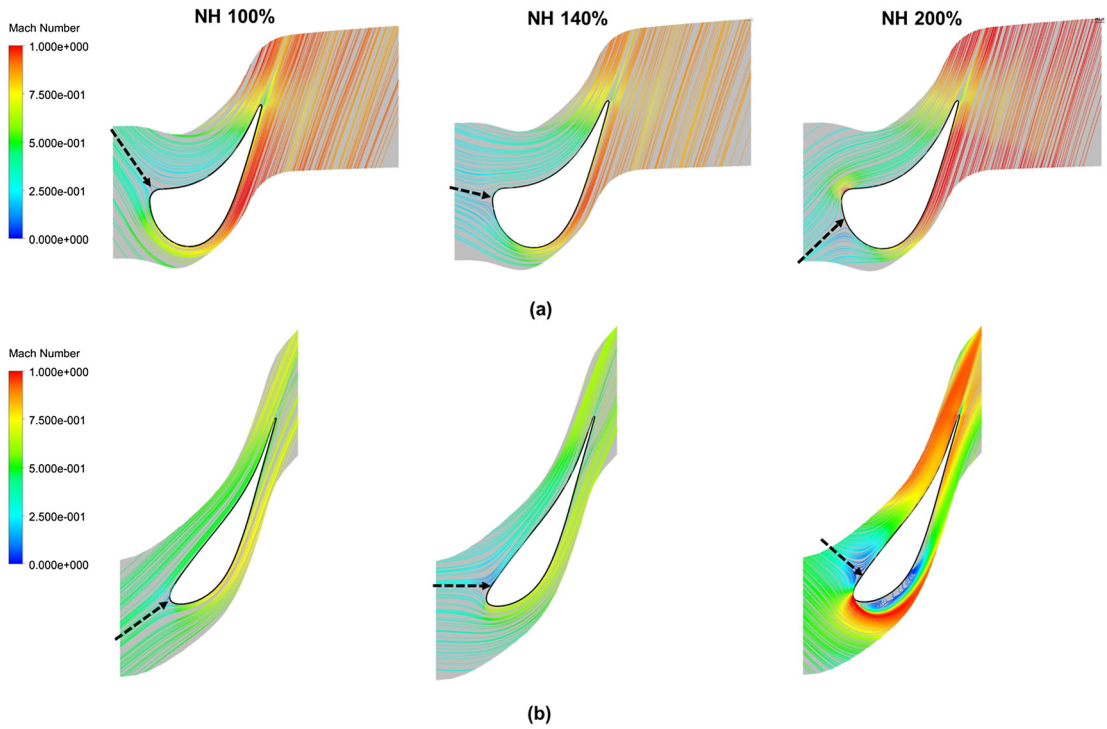


Fig. 7. Streamlines with arrows showing mean flow direction – (a) HP rotor mid plane relative Mach number, (b) IP stator mid plane absolute Mach number.

parallel to the engine axis, and, thereafter continues to increase in the direction that is in opposite sense to the blade inlet angle of the rotor aerofoil. Consequent to this change in the direction and magnitude of the relative inlet velocity to the rotor the static pressure field at the inlet plane of the rotor changes in such a way that the total-to-static pressure ratio across the HP stator initially decreases until the 140% speed line and then increases. The total to static pressure ratio across the HP stator passage is clearly proportional to the mass flow passing through the stator passages. In the present case, since the trailing edge coolant ejection is also modelled, the minimum area in the HP stator passage depends on the interaction between the coolant flow and the hot gases in the main flow path. The change in the static pressure at the exit of stator is sensed by both the coolant flow and the main flow. Therefore the interaction between the flows that are expanding to the same static pressure result in variations in the minimum area that consequently is responsible for the trend of the mass flow function of the HPT with speed. However, it is to be noted that this change in the mass flow function is within 1% of the mass flow at the nominal operating condition of the turbine. It is to be noted that as the speed function increases the pressure at which the turbine chokes also shows a trend similar to the variation of mass flow function for the same reason as above. The change in the flow streamlines at the HP rotor mid plane that results in changes in the static pressure field with angular velocity is shown in Fig. 7(a).

The map of the IPT is generated corresponding to each operating point in the HPT characteristic. It is seen that at a fixed non-dimensional speed of the IPT and the HPT, as the expansion ratio of the IPT increases, the mass flow function increases until the choking value and remains constant as is typical in turbines. However, at the same non-dimensional speed of the IPT, a change is observed in the mass flow function of the IPT when there is a change in the non-dimensional speed function of the HPT. The change in the IPT mass flow function is minimal up until a HPT speed of 140%. There is a progressive reduction in the IP mass flow function beyond a HPT speed of 140%. The reason for this reduction in the mass flow function is primarily because of the change in the property of the flow that is entering the IP stator from the HPT rotor outlet. As the non-dimensional speed function increases, the direction of the absolute velocity vector at the HP rotor outlet becomes increasingly different from that of the metal angle at the entry of the IP stator. Therefore, the incidence angle at the IP stator inlet becomes higher with increase in the non-dimensional speed of the HPT, and eventually beyond a speed of 140%, the flow breaks down and leads to reduction in the flow capacity in the IP stator passages. For each operating point of the HPT, the expansion ratio of the IPT is fixed from mass flow matching of the two stages. The reduction in the swallowing capacity of the IPT is beneficial in restricting the terminal speed obtained by the HPT since the lower mass flow function of the downstream IPT stage will lead to a downward shift in the operating expansion ratio of the HPT that will consequently reduce the torque produced by the rotor. The change in the flow streamlines at the IPT mid plane is shown in Fig. 7(b).

5.2. Characteristics at different axial displacements and worn fins in the tip seal

Rearward movement of the HPT rotor leads to an increase in the HP stator–rotor gap, opening of the tip seal and rim seal gaps. Further opening of the tip seal gap occurs when the fins of the shroud tip are worn. This leads to changes in the flow behaviour in the turbine stages and consequently to degradation in the performance of the turbine at each expansion ratio and non-dimensional speed function. The variation of HPT torque with axial displacement at the reference pressure ratio for the case with and without damage in the tip seal domain for different speed functions are shown in Fig. 8. Similarly, Figs. 9 and 10 show the comparison of HPT and IPT mass flow functions for both the cases. In all these figures in the graphs for the worn fins case, the values of the case with no damage is shown in the background for quick comparison.

The torque produced by the HP rotor decreases with an increase in axial displacement for all non-dimensional speed functions. The reduction in torque for the intact seal case is 10%, while with worn

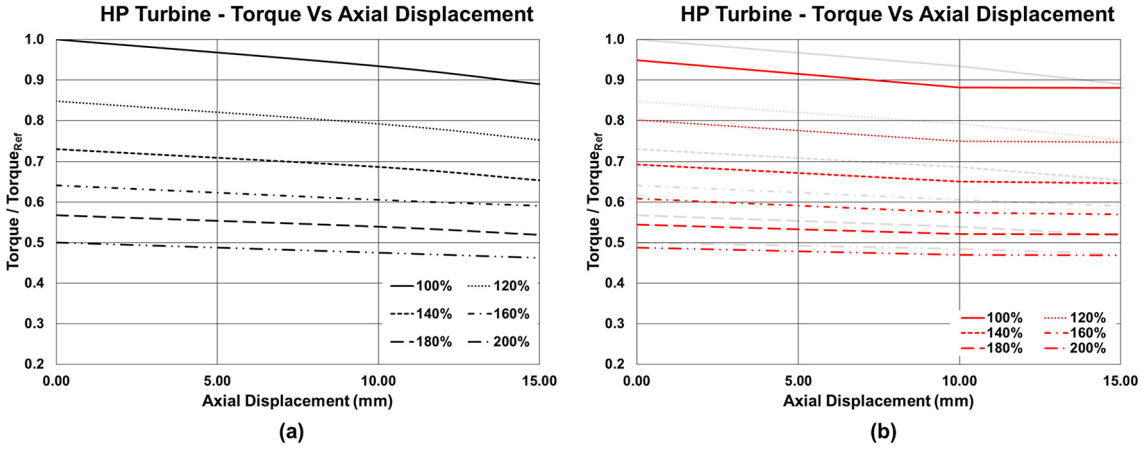


Fig. 8. HPT torque vs axial displacement at reference pressure ratio. (a) No damage in tip seal fins. (b) Worn tip fins.

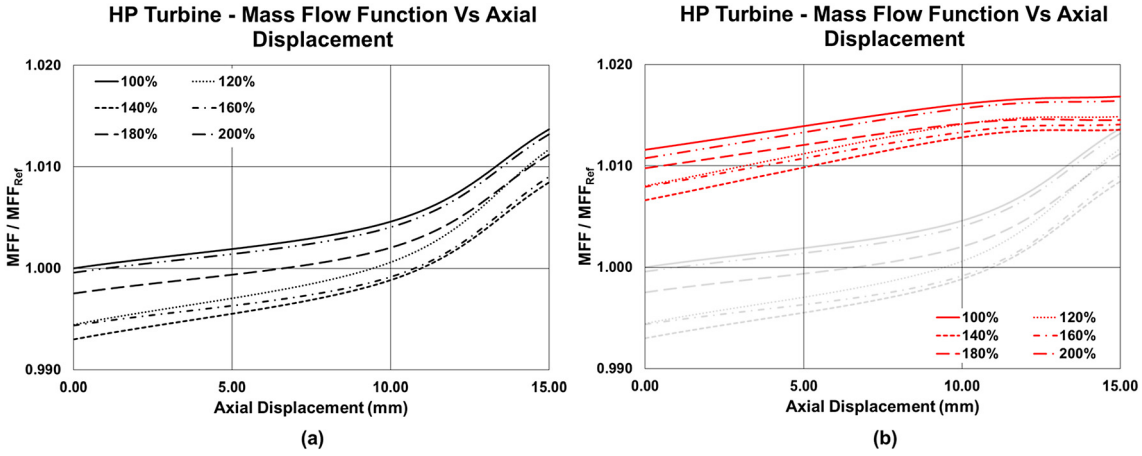


Fig. 9. HPT mass flow function vs axial displacement at reference pressure ratio. (a) No damage in tip seal fins. (b) Worn tip fins.

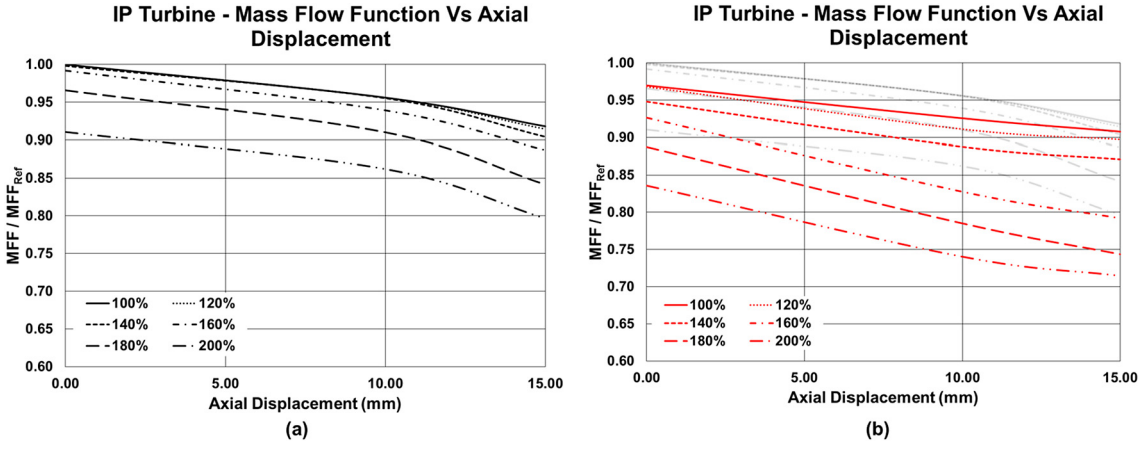


Fig. 10. IPT mass flow function vs axial displacement at reference IP pressure ratio. (a) No damage in tip seal fins. (b) Worn tip fins.

seals this value is 5%. This degradation in torque is mainly because of the change in the static pressure distribution in the rotor aerofoils brought about by the increasing migration of the flow from the aerofoil passages to the tip gap because of the opening of tip clearances. The change in static pressure distribution in the rotor aerofoils is such that the resultant force acting on the aerofoil decreases with increasing axial displacement that consequently leads to a reduction in the torque. The torque produced by the rotor in the case of worn fins in the tip seal is lower than the configuration without damage because of further increase in mass flow migration caused by the destruction of the fins in the tip seal domain that controls the clearances. Fig. 11 shows the representative change in static pressure distribution at different axial displacements for a typical operating point. The degradation in the torque between the 10 mm and 15 mm displacement locations for the worn fins case is not significant because as the rotor moves rearward, the geometry of the casing and the flare of the rotor is such that when there are no fins in the tip seal domain, the change in the minimum clearance area in the tip seal does not change significantly between the two displacement locations. However, this

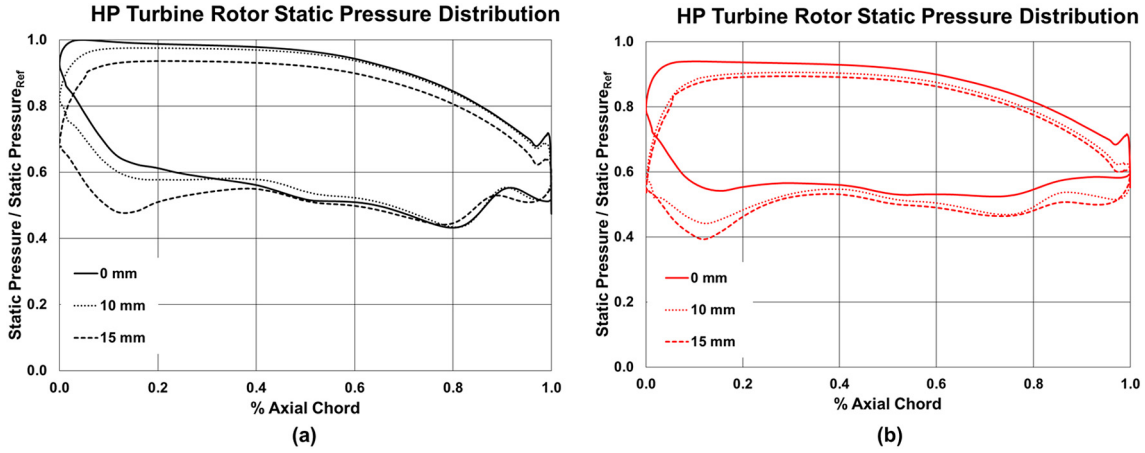


Fig. 11. Static pressure distribution in rotor tip aerofoil at different axial displacement locations. (a) No damage in tip seal fins. (b) Worn tip fins.

is not the case for the tip seal with fins in which as the displacement increases, the minimum clearance area increases. It is also noticed that the reduction of torque with displacement becomes less pronounced with increase in non-dimensional speed function. This is because, as the speed function increases, the static pressure distribution in the rotor becomes increasingly influenced by the increasing deviation of the direction of the flow vector into the rotor, and to a lesser extent by the pressure differential arising from mass flow migration to the tip seal.

The mass flow function of the HPT increases by almost 1.5% with an increase in axial displacement for all non-dimensional speed functions. The increase in stator–rotor gap of the HPT with axial displacement results in change in the potential interaction between the aerofoil rows such that the blockage to the stator exit flow becomes lower. Migration of the flow to the tip through zones of entrainment also results in a reduction of the static pressure at the rotor inlet plane. These two factors combine to increase the 'total-to-static' pressure ratio of the HP stator that increases the mass flow through the stator passages. Clearly in the case of worn fins the static pressure at the rotor inlet will be lower because of higher amount of mass flow migration through the tip, and therefore the mass flow function of the HPT with worn fins is higher than that of the undamaged configuration. As explained before, since the increase in mass flow migration to the tip is minimal between 10 mm and 15 mm displacements for the worn seal, the change in the static pressure at the rotor inlet is also minimal, and hence the mass flow function increase is also not significant in the worn fins for these displacements as in the undamaged case, being higher by 0.5%. However, it is to be noted that the entire extent of the variation mass flow function of the HPT for both the cases at all axial displacements is within 1%.

The mass flow function of the IPT decreases with increase in axial displacement for all the HPT rotor non-dimensional speed functions, by nearly 10% at 200% NH. As explained above, the proportion of the flow through the tip seal increases with axial displacement. The flow that constitutes the tip leakage is not expanded, accelerated and turned to the same extent as the flow in the rotor passages. Therefore the flow at the entry to the IP stator near the tip is increasingly at a higher total pressure, lower velocity and points in a direction that is different from the rotor metal inlet angle. Consequently there are flow separations, and stronger flow accelerations near the tip region of the IP stator that increases the losses in the IP stator passages and leads to a reduction in the mass flow function of the IPT stage. The reduction in the mass flow function is clearly much higher in the case of the worn fins configuration because of the higher amount of tip leakage. In the case of the undamaged configuration the drop in the mass flow function becomes considerable after a non-dimensional speed function of 160%. This is because the rounded leading edges of the IP stator vane are able to operate insensitive of the change in flow direction because of increase in speed. However, in the case of the worn fins, considerable reduction is observed beyond a speed function of 120%. This is because the increasing change in the flow direction near the tip of the IP stator entry by a larger amount of tip leakage flow is beyond the range in which the leading edges are able to be insensitive. As observed in the other characteristics, the change between the 10 mm and 15 mm configuration in the worn fins case is smaller. At 15 mm displacement the IPT mass flow function is reduced by 2.5%. Detailed discussion of the flow physics at different axial displacements for the case with no damage and with worn fins are described in separate publications by the authors that focus on interpretation of the flow phenomena and its effect on the turbine parameters [2,3].

6. Conclusions

The hi-fidelity characterisation of the HPT and IPT in terms of the parameters relevant for the prediction of the terminal speed of the overspeeding rotor in a HP shaft failure prediction model is described in detail in the present work. The HP rotor torque, HPT mass flow function and the IPT mass flow function variation for a range of expansion ratios in the non-dimensional speed function range of 100% to 200% of the nominal value is obtained from 3D CFD analyses. The computational domain of the HPT includes the trailing edge coolant flows, rim seal and tip seal leakage flows to accurately capture the flow physics in the over-speeding turbine stage. The characteristics are generated at different axial displacement locations i.e. 0 mm, 10 mm and 15 mm, to accurately capture the change in the characteristic parameters of the turbine with the rearward axial displacement of the rotor sub-assembly during the development of the over-speed event, as predicted from a validated thermo-mechanical friction model built from non-linear structural dynamic analyses. The rearward movement of the rotor leads to changes in the properties of the leakage flow that interacts with the main stream and this change is predicted from a transient secondary air system model and incorporated in the computational model. At the undisplaced location, the HP rotor torque decreases with non-dimensional speed function, the IPT mass flow function remains nearly similar until a non-dimensional speed function of 140% and then decreases considerably, and the HP turbine mass flow function decreases until a non-dimensional speed function of 160% and then increases. As the rotor gets axially displaced, the HP rotor torque and IPT mass flow function decreases by nearly 10%, and the HPT mass flow function increases by nearly 1.5% with

respect to the undisplaced configuration at each speed function. The characteristics of the turbines at different axial displacement locations will improve the accuracy of prediction of the terminal speed of the overspeeding rotor by providing the proper trends of the change in the turbine performance characteristics with displacement. Whilst not shown here characteristic maps for different IP speeds were also created, exhibiting similar trends, allowing integration into a performance model.

An additional set of characteristics are generated at different axial displacements for the case in which the rotor shroud tip fins are damaged following the shaft failure. It is observed that at 0 mm and 10 mm axial displacements the values of the HP torque and IPT mass flow function are lower by 5%, and the HP turbine mass flow function is higher by 1% compared to the undamaged configuration. At 15 mm axial displacement, the HP torque and IPT mass flow functions are lower by 2.5%, and the HPT mass flow function is higher by 0.5%. Therefore, damage to the tip of the rotor results in degradation of the parameters that influence the terminal speed of the rotor, and design modifications in the turbine shaft that can lead to quick displacement up to 10 mm of the rotor sub-assembly may hold potential for reducing the terminal speed of the rotor.

Conflict of interest statement

The authors declare that there is no conflict of interests regarding the publication of this article.

Acknowledgements

The authors would like to express their gratitude to Rolls-Royce plc. for supporting this research and for permission to publish the paper.

References

[1] VV. AA., Certification Specifications for Engines. CS-E – Amendment 3, Technical report, European Aviation Safety Agency, 2010.
[2] VV. AA., Certification Memorandum – Turbine Over-Speed Resulting from Shaft Failure, Technical report, European Aviation Safety Agency, 2012.
[3] C. Soria, Gas Turbine Shaft Overspeed/Failure Performance Modelling, Doctoral dissertation, Cranfield University, 2014.
[4] L. Gallar, Gas Turbine Shaft Overspeed/Failure Performance Modelling, Doctoral dissertation, Cranfield University, 2010.
[5] A. Psarra, V. Pachidis, P. Pilidis, Finite element turbine blade tangling modelling following a shaft failure, in: ASME Turbo Expo 2009: Power for Land, Sea, and Air, American Society of Mechanical Engineers, January 2009, pp. 73–81.
[6] B. Yang, Blade containment evaluation of civil aircraft engines, Chin. J. Aeronaut. 26 (1) (2013) 9–16.
[7] M. Haake, R. Fiola, S. Staudacher, Multistage compressor and turbine modelling for the prediction of the maximum turbine speed resulting from shaft breakage, J. Turbomach. 133 (2) (2011) 021022.
[8] L. Pawsey, D. John, V. Pachidis, Turbine overspeed – on the aerodynamic performance of an unlocated HP turbine rotor, Aeronaut. J. 121 (1242) (August 2017), The International Society of Air-Breathing Engines (ISABE) Special Issue.
[9] L. Pawsey, D. John, V. Pachidis, Turbine overspeed – on the aerodynamic performance of an unlocated HP turbine rotor with worn fins in the tip seal, in: ASME Turbo Expo Power 2017, North Carolina, USA, June 2016, GT2017-64312.
[10] A. Gonzalez, V. Pachidis, On the numerical simulation of turbine blade tangling after a shaft failure, in: ASME Turbo Expo 2014: Turbine Technical Conference and Exposition, American Society of Mechanical Engineers, June 2014, V07BT33A026.
[11] L. Gallar, C. Calcagni, V. Pachidis, P. Pilidis, Development of a one-dimensional dynamic gas turbine secondary air system model—part I: tool components development and validation, in: ASME Turbo Expo 2009: Power for Land, Sea, and Air, American Society of Mechanical Engineers, January 2009, pp. 457–465.
[12] C. Calcagni, L. Gallar, V. Pachidis, Development of a one-dimensional dynamic gas turbine secondary air system model—part II: assembly and validation of a complete network, in: ASME Turbo Expo 2009: Power for Land, Sea, and Air, American Society of Mechanical Engineers, January 2009, pp. 435–443.
[13] P.J. Roache, Verification and Validation in Computational Science and Engineering, Hermosa, 1998.
[14] ANSYS, C.F.X., ANSYS CFX-solver theory guide. ANSYS CFX Release, 11, 2012, pp. 69–118.
[15] F.R. Menter, Review of the shear-stress transport turbulence model experience from an industrial perspective, Int. J. Comput. Fluid Dyn. 23 (4) (2009) 305–316.



https://dspace.org/

Characterisation of turbine behaviour for an engine overspeed prediction model

Pawsey, Lucas; Rajendran, David John; Pachidis, Vassilios

2017-11-28
Elsevier
https://doi.org/10.1016/j.ast.2017.11.037
Pawsey L, Pachidis V, Rajendran DJ. (2018) Characterisation of turbine behaviour for an engine overspeed prediction model. Aerospace Science and Technology, Volume 73, February 2018, pp. 10-18

Downloaded from a DSpace repository. https://dspace.org/